Particles I

Access the latest eBook →

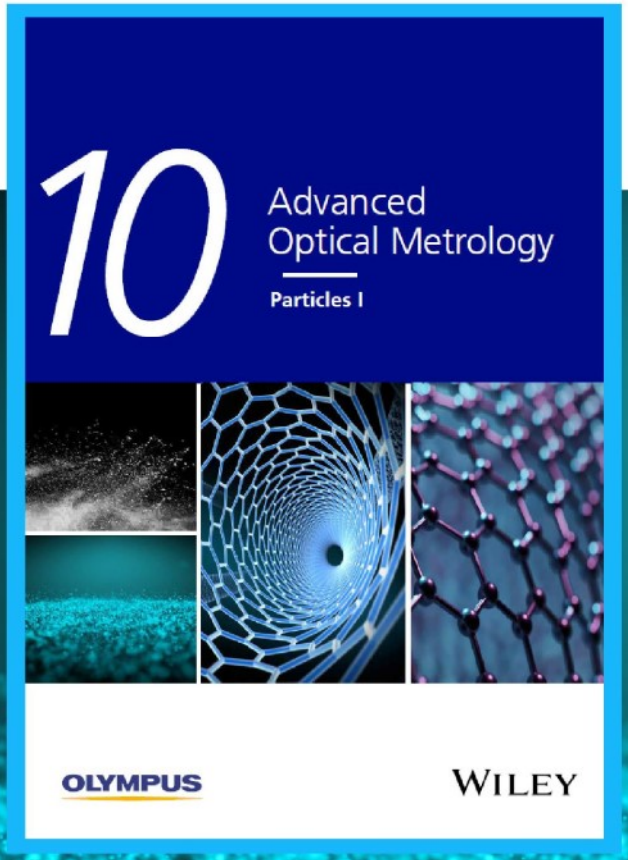

Particles: Unique Properties, Uncountable Applications

Read the latest eBook and better your knowledge with highlights from the recent studies on the design and characterization of micro- and nanoparticles for different application areas.

Access Now

This eBook is sponsored by

OLYMPUS

WILEY

ADVANCED MATERIALS

www.advmat.de

Biomaterial-Based "Structured Opals" with Programmable Combination of Diffractive Optical Elements and Photonic Bandgap Effects

*Yu Wang, Wenyi Li, Meng Li, Siwei Zhao, Fabio De Ferrari, Marco Liscidini, and Fiorenzo G. Omenetto**

Naturally occurring iridescent systems produce brilliant color displays through multiscale, hierarchical assembly of structures that combine reflective, diffractive, diffusive, or absorbing domains. The fabrication of biopolymer-based, hierarchical 3D photonic crystals through the use of a topographical templating strategy that allows combined optical effects derived from the interplay of predesigned 2D and 3D geometries is reported here. This biomaterials-based approach generates 2D diffractive optics composed of 3D nanophotonic lattices that allow simultaneous control over the reflection (through the 3D photonic bandgap) and the transmission (through 2D diffractive structuring) of light with the additional utility of being constituted by a biocompatible, implantable, edible commodity textile material. The use of biopolymers allows additional degrees of freedom in photonic bandgap design through directed protein conformation modulation. Demonstrator structures are presented to illustrate the lattice multifunctionality, including tunable diffractive properties, increased angle of view of photonic crystals, color-mixing, and sensing applications.

The hierarchical assembly of natural materials that generate iridescences have been the subject of intense research to understand their assembly, structure, function, and to mimic their performance. These structures whose features range from the nano- to the macroscale are often developed by finely selected self-assembly processes using a limited set of simple building blocks, which manifest in the form of diffraction gratings, multilayer interference stacks, photonic crystals, diffusers, or other optical structures.[1] A variety of striking optical effects, such as iridescence,[2] angle-independent coloration,[3] polarization,[4] complex color mixing,[5] antireflection,[6] ultra-blackness,[7] ultra-whiteness,[8] light focusing,[9] and dynamic structural color,[10] result from these unique, naturally occurring material system. In addition to coloration, such hierarchical photonic structures also add further functional utility such as superwettability,[11] selective vapor responses,[12] or light trapping.[13]

These complex photonic architectures over multiple length scales provide inspiring examples for the fabrication of synthetic counterparts that attempt to mimic their structure, optical property, and function,[14] driving new generation of photonic devices for a wide range of applications, including sensing, displays, security, wetting, photovoltaics, aesthetics, and others.[15] To date, considerable progress has been made in forming various bioinspired hierarchical photonic structures.[16] Coupling of diffraction gratings with other optical element, such as multilayer,[16a,c,f] 3D photonic crystals,[17] thin films,[18] or diffraction gratings,[16g] has been a recurring theme for this purpose. However, integrating structural hierarchy, order/disorder, multiple optical elements, and multiple functions into a single photonic material using simple building blocks is still an open challenge.

We present here a biomaterials-based approach for the construction of hierarchical 3D photonic structures (composites of 2D diffractive micropatterns and 3D photonic nanostructures) that integrate multiple optical functions in a single material, by leveraging a combination of protein self-assembly,[19] colloidal assembly, and top-down transformation techniques. Demonstrator free-standing structures that combine structural color, diffusion, diffraction within the same optical element are shown. The resulting composites can be programmably modulated (i.e., stop-band and diffraction tuning) through controlling the layer numbers and lattice constants of assembled

Dr. Y. Wang, W. Li, M. Li, Dr. S. Zhao, F. De Ferrari, Prof. F. G. Omenetto
Department of Biomedical Engineering
Tufts University
4 Colby Street, Medford, MA 02155, USA
E-mail: Fiorenzo.Omenetto@tufts.edu
Dr. Y. Wang, W. Li, M. Li, F. De Ferrari, Prof. F. G. Omenetto
Silklab
Tufts University
200 Boston Avenue, Medford, MA 02155, USA
Prof. M. Liscidini
Dipartimento di Fisica
Università degli Studi di Pavia
via Bassi 6, 27100 Pavia, Italy
Prof. F. G. Omenetto
Department of Physics
Tufts University
4 Colby Street, Medford, MA 02155, USA
The ORCID identification number(s) for the author(s) of this article can be found under https://doi.org/10.1002/adma.201805312.

DOI: 10.1002/adma.201805312

colloidal crystals and reconfigured through contact-less UV light and water vapor (WV) exposure. Potential applications that rely on co-located functions are illustrated by combining diffusers with photonic crystals for wide viewing angle, multicolor patterned displays, and by developing combined photonic bandgap/diffraction-based sensors.

The fabrication of hierarchical 3D photonic structures is achieved through a facile and scalable manufacturing scheme that relies on colloidal assembly. The latter is widely adopted as a facile and economical technique for bottom-up fabrication of 3D photonic structures.[20] To date, several top-down fabrication methods, such as lithography,[17a,21] microimprinting,[22] or printing,[23] have been combined with colloidal self-assembly to design hierarchical 3D structures. These approaches can be time-consuming, uneconomical, and challenging when additional complexities are introduced in the 3D structures at multiple length scales. Biological templating has provided an efficient route to reproduce the intricate 3D structure found in natural structures,[24] but is limited in reproducibility and scale-up, thereby hindering practical applications. On the contrary, topographical templating coupled with colloidal self-assembly offers a cost- and time-effective approach for the generation of large-scale and complex 3D hierarchical structures,[20,25] providing a promising pathway to build composite photonic structures.

The formation of hierarchical photonic structures is based on the use of polystyrene (PS) colloidal crystal multilayers on patterned surfaces as templates. The resulting structures have three scale-dependent optical responses, namely: i) a photonic crystal behavior derived from the nanoscale periodicity of the optical lattice, ii) the diffractive behavior from the microscale patterning, and iii) light gathering/processing ability derived from the multi-centimeter size of the devices. A schematic of the fabrication process is shown in **Figure 1**a. A crystalline PS nanosphere monolayer at the water/air interface,[26] generated through the direct self-assembly of PS nanospheres (diameters of 210 or 300 nm) is transferred onto predesigned diffractive surfaces to form templated, close-packed PS colloidal crystal monolayers. The transfer process is repeated ultimately providing a template lattice with a controllable number of layers.[27] An aqueous solution of silk fibroin is then cast into the lattice and allowed to solidify into a free-standing film. The PS nanospheres are then removed by dissolution in toluene generating an amorphous (non-crosslinked)[28] free-standing silk inverse opal lattice presenting both structural color and diffractive behavior or "hierarchical opals" (HOPs).

HOPs were generated by using three kinds of commercially available (Digital Optics/Tessera Inc., San Jose, CA, USA), Diffractive Optical Elements (DOEs) as templates: a diffuser, a pattern generator (PG), and a grating (Figure S1, Supporting Information). The resulting HOPs are labeled as Diffuser-HOP, PG-HOP, and Grating-HOP to represent the DOE function associated with the photonic crystal lattice. The combination of DOEs and 3D inverse colloidal crystal offers expanded optical utility through their functional interplay. Specifically, embedding 3D nanoscale photonic structure reconfigures the diffraction of the 2D optical elements, while the DOE topography influences the structural color appearance at different angles. It should be mentioned that both the diffuser and PG are used as diffusive templates, but with different far-field diffraction patterns and thus different 2D micropattern designs (Figure S1, Supporting Information). Scanning electron microscope (SEM) images of the prepared silk HOPs are shown in Figure 1b–d, and Figure S2 in the Supporting Information. At the microscale, HOPs can fully replicate the microstructures of the corresponding substrate. At the nanoscale, they all show the ordered hexagonal arrays of air cavities (where the PS spheres were originally located) while displaying the ability to effectively replicate the surface patterns used as the template, as shown by the grating with $d = 600$ lines mm^{-1} and groove depth of 450 nm observed in the atomic force microscopy (AFM) images and cross-section profiles (Figure 1h–j and Figure S1d, Supporting Information). The mismatch between the dimension of the nanoparticles and the grating period can cause some edge irregularities in the end structures which results in the slight mismatch in depth and width of the colloidal assembly (Figure 1i,j). The lattice constant ($\wedge$), defined as the center-to-center distance of the air cavities, is the same as the diameter of PS sphere used, i.e., $\wedge = 300$ nm (Figure 1b–d) and $\wedge = 210$ nm (Figure S2, Supporting Information), respectively. The cross-sectional SEM images of HOPs (Figure 1e–g) display the coexistence of microscale and nanoscale features with the patterned diffractive structure and the inverse photonic lattice both clearly visible. The fidelity of these free-standing constructs is enabled by the material characteristics of silk fibroin, which on top of its favorable optical properties,[19,29] in general, includes its robust mechanical properties and nanoscale processability. All the HOPs considered here are three-layered inverse colloidal crystals with a lattice constant of 300/210 nm, unless otherwise noted.

The presence of 2D microscale and 3D nanoscale patterns allows for the integration of different optical properties in a single, biocompatible matrix. The nanoscale periodic lattice structure of HOPs is responsible for the material's structural color as previously shown for silk inverse opals.[28a,29] The total reflectance spectra of both Diffuser-HOP and PG-HOP clearly show reflective stop-band peaks centered at $\lambda = 585$ nm (**Figure 2**a,b), and $\lambda = 420$ nm (Figure S3, Supporting Information) for $\wedge = 300$ nm and $\wedge = 210$ nm, respectively. These stop-band positions fit in well with those of silk inverse opals with the same lattice constant and refractive index (RI) ($n = 1.54$ at 633 nm, Figure S4, Supporting Information),[28a] further indicating highly ordered hollow silk fibroin structure even on patterned surface. Expectedly, these high reflectance regions are more efficient with the increase of layer numbers of the inverse colloidal crystals (Figure S5, Supporting Information).

The bright structural color appearance (inserts in Figure 2a,b) derives from the interaction between the 3D nanoscale photonic lattice and the 2D microscale patterns. The concomitant introduction of microscale patterns can not only modulate the structural color of HOPs, but maintain the performance of the DOEs with the added utility of the interplay between reflective and diffusive/diffractive functionality. The far-field diffraction patterns in both reflection and transmission obtained by propagating a laser beam through the HOPs (as schematically shown in Figure 1k) are shown in Figure 2c–f along with the AFM images of the inverse opals' diffractive surfaces. Additional functionality is illustrated in Figure 2g, which shows the images produced when an object (i.e., the word "Tufts" from an LCD display) is viewed through different HOPs.

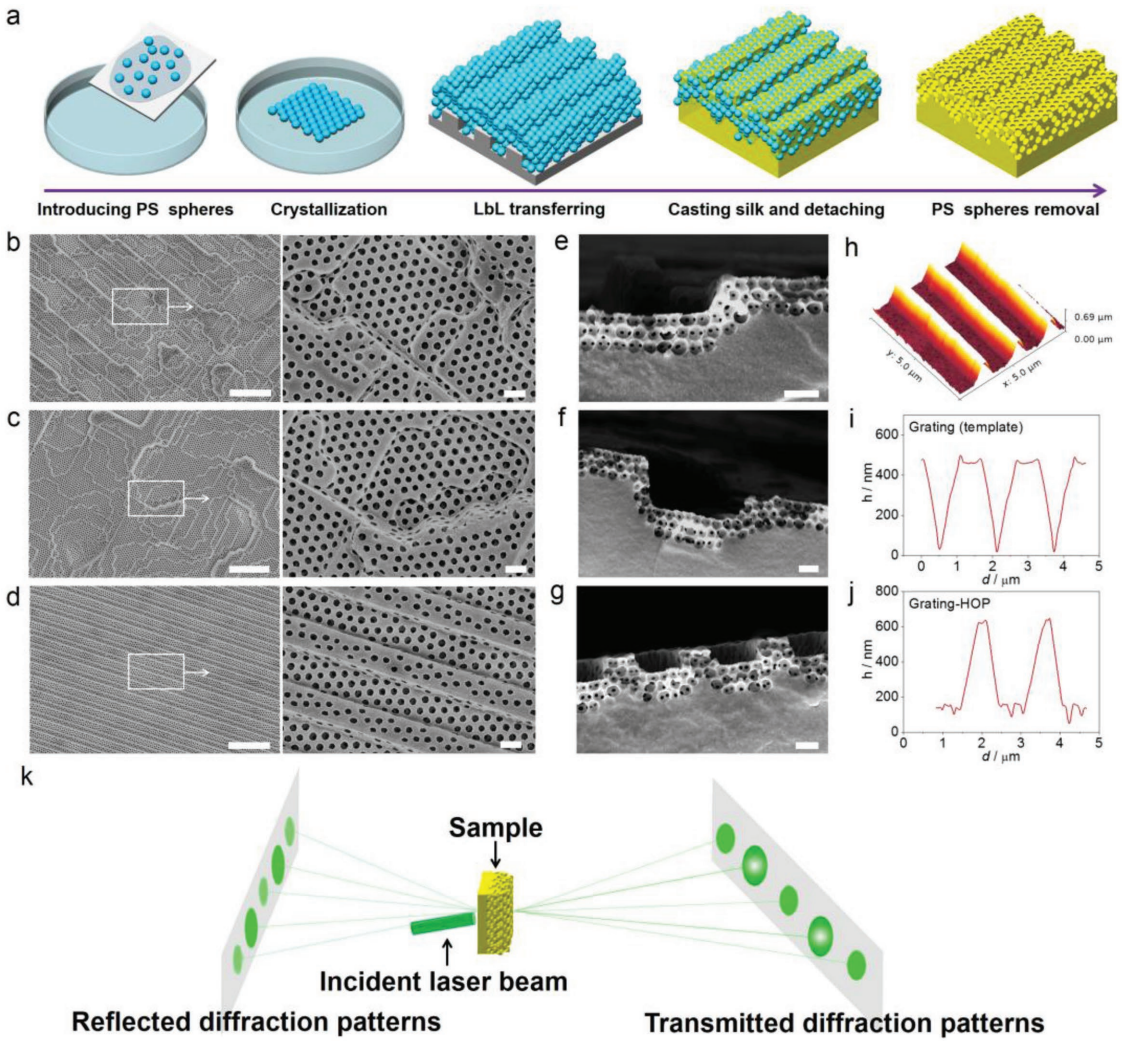

Figure 1. Formation of hierarchical photonic structures. a) General schematic of the fabrication process. Left to right: introducing monodisperse PS nanospheres to water surface; crystallization at the water/air interface; forming hierarchical PS colloidal crystals with controllable layers through layer-by-layer transferring the crystalline monolayer to patterned substrate; casting silk solution into the template and drying to generate patterned silk/PS composite; removing PS nanospheres to attain hierarchical inverse colloidal crystal. b–g) Typical surface (b–d) and cross-sectional (e–g) SEM images of HOPs formed by using templates of colloidal crystals composed of PS spheres with diameter of 300 nm on different topographically patterned substrates: (b,e) diffuser (Diffuser-HOP), (c,f) pattern generator (PG-HOP), and (d,g) grating (Grating-HOP). h–j) Replication process of Grating-HOP showing an AFM image of the 2D diffractive surface (h), the cross-section profile of the 2D diffractive surface used as the template (i), and the replicated inverse opal profile (j). k) General schematic of the performance of the Grating-HOP structure. Scar bars in (b–d): 5 μm (left), 500 nm (right). Scar bars in (e–g): 500 nm.

As shown in Figure 2h and 2i, the image is either defocused or diffracted by the Diffuser-HOP and Grating-HOP, respectively, indicating the preservation of the optical function caused by the templating and replication of sub-micrometer topographies.

While the far-field intensity distribution of a DOE depends on its surface structure (e.g., height and periodicity), transparency, and effective RI, both the reflective and transmissive contributions can be modulated by tuning the photonic bandgap associated with the inverse colloidal crystal lattice. As such, the number of layers in the colloidal photonic crystal will determine the optical interplay in the HOP structures. The effect of the photonic crystal lattice on the diffractive properties of PG-HOPs and Diffuser-HOPs was evaluated (**Figure 3**a and Figure S7, Supporting Information) by comparing the far-field intensity of the diffracted orders of a HOP and an identical diffractive structure without the photonic crystal lattice. The laser wavelength was selected to match the stop-band peak position to enhance the contribution due to the photonic crystal lattice. As shown in Figure 3b (and Figures S6 and S7, Supporting Information), the reflected diffraction intensity increases, while the transmitted diffraction intensity decreases in correspondence of the increase in the number of lattice layers due to the enhanced reflectivity from photonic crystal leading to higher diffraction efficiencies. This is also illustrated in Figure 3c, where the reflected first-order diffraction efficiency from Grating-HOPs increases with the number of lattice layers when the stop-band matches the laser wavelength, while the transmitted diffraction efficiency decreases.

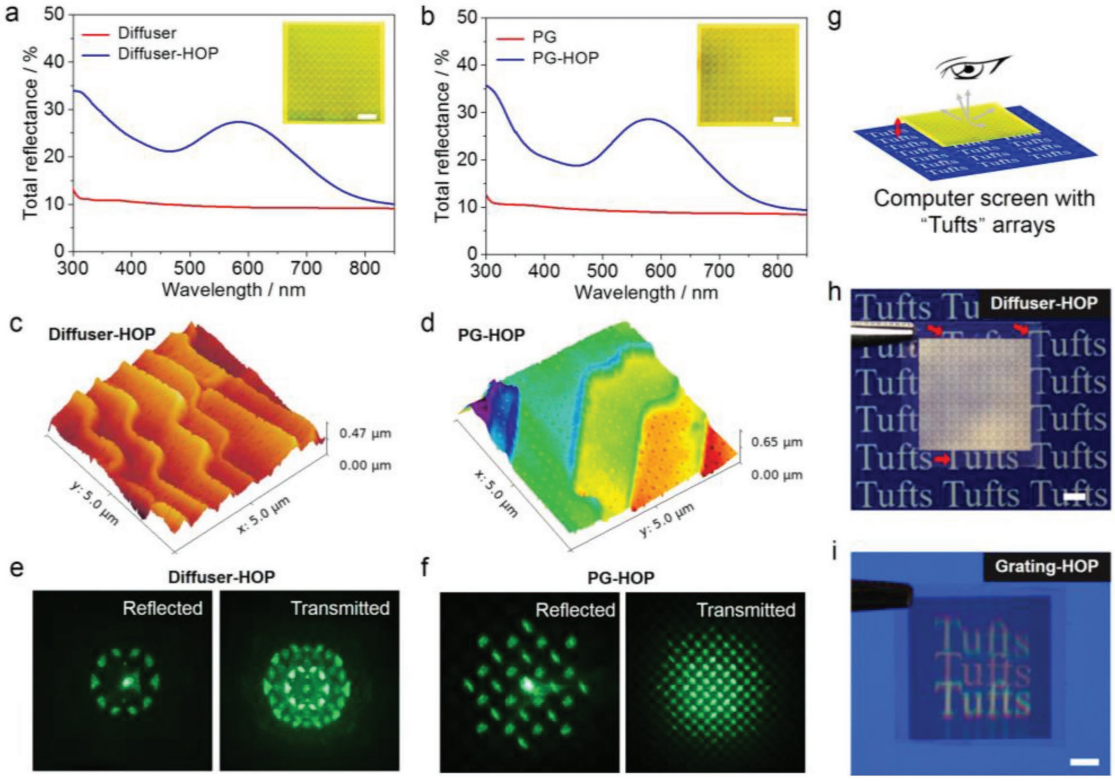

Figure 2. Integration of structural color and diffraction. a,b) Total reflectance spectra of Diffuser-HOP (a) and PG-HOP (b) with $\wedge = 300$ nm. The spectra of corresponding 2D optical elements are also shown for comparison. Inserts: photographs showing vivid structural colors. Scale bars: 2 mm. c,d) Corresponding 3D AFM images of Diffuser-HOP (c) and PG-HOP (d). e,f) The projected diffraction patterns in both reflection and transmission modes obtained from propagation of a green laser ($\lambda = 543.5$ nm) through Diffuser-HOP (e) and PG-HOP (f). g) Schematic of the experimental setup to generate transmitted images of the "Tufts" words through HOPs. The red double arrow indicates the separation between the actual image and the sample. h,i) Corresponding transmitted images of the "Tufts" words through Diffuser-HOP (h) and Grating-HOP (i) with $\wedge = 300$ nm. The arrows in (h) indicate the visible letters through silk inverse opal film. In (i), the "Tufts" word in the middle is diffracted to both sides by Grating-HOP. Scale bars: 2 mm.

Tuning the stop-band of the photonic crystal introduces an additional degree of spectral selectivity on the diffractive structure that templates the lattice, which in turn can provide tunability and selectivity over the diffracted pattern from the structure. The influence of the lattice constant on the diffractive properties of HOPs was first examined by assembling HOPs with different lattice constants $\wedge$. Tuning the photonic lattice influences the extraction efficiency of specific wavelengths[29,30] and allows one to enhance the intensity of diffracted spectral components in reflection when the laser wavelength matches the stop-band peak position. This is confirmed by the measurements shown in Figure 3d, where illumination by a blue laser ($\lambda = 405$ nm) causes the structure with $\wedge = 210$ nm to display higher reflected diffraction intensity than the corresponding structure with $\wedge = 300$ nm, while reflected intensities are lower for the $\wedge = 210$ nm lattice compared to the structure with $\wedge = 300$ nm spacing when the structure is illuminated by a green laser ($\lambda = 543.5$ nm). Expectedly, the transmitted diffraction intensities correlate with what observed above (Figure S8, Supporting Information). Similarly, Grating-HOPs with $\wedge = 210$ nm show lower +1st order reflected diffraction efficiency and then higher transmitted diffraction efficiency than the corresponding structure with $\wedge = 300$ nm when illuminated by a green laser (Figure 3c) due to the mismatched wavelength between laser and stop-band peak.

One of the advantages of using biopolymers, and specifically silk fibroin, is the ability to induce controllable conformational changes in the amorphous matrix of the material through the rearrangement of the fibroin molecular chains.[28] This is achieved by using either UV or WV to modify the photonic lattice of silk inverse opal and allowing for programmable structural color tuning. This unique feature applies to the HOPs presented here (Figure S9a–d, Supporting Information), where the same strategy can be adopted to provide photonic lattice tuning and further rational design of the material's spectral response. The (irreversible) reconfiguration of the photonic lattice by UV or WV allows further degrees of freedom in the design of 2D/3D optical structures allowing for multispectral optimization of the diffracted/transmitted/reflected spectral components and their interplay. Figure 3e,f shows an example of hierarchical structures modulation caused by UV or WV treatment on the diffraction performance of the HOPs. Conformational changes in the lattice result in controllable variations of the diffraction intensity, consistent with the associated change in reflection intensity because of photonic crystal lattice modulation (Figure 3e,f and Figure S9c,d, Supporting Information). It is observed that while the lattice constant can be tuned, the surface micropatterns are almost unaffected after either UV

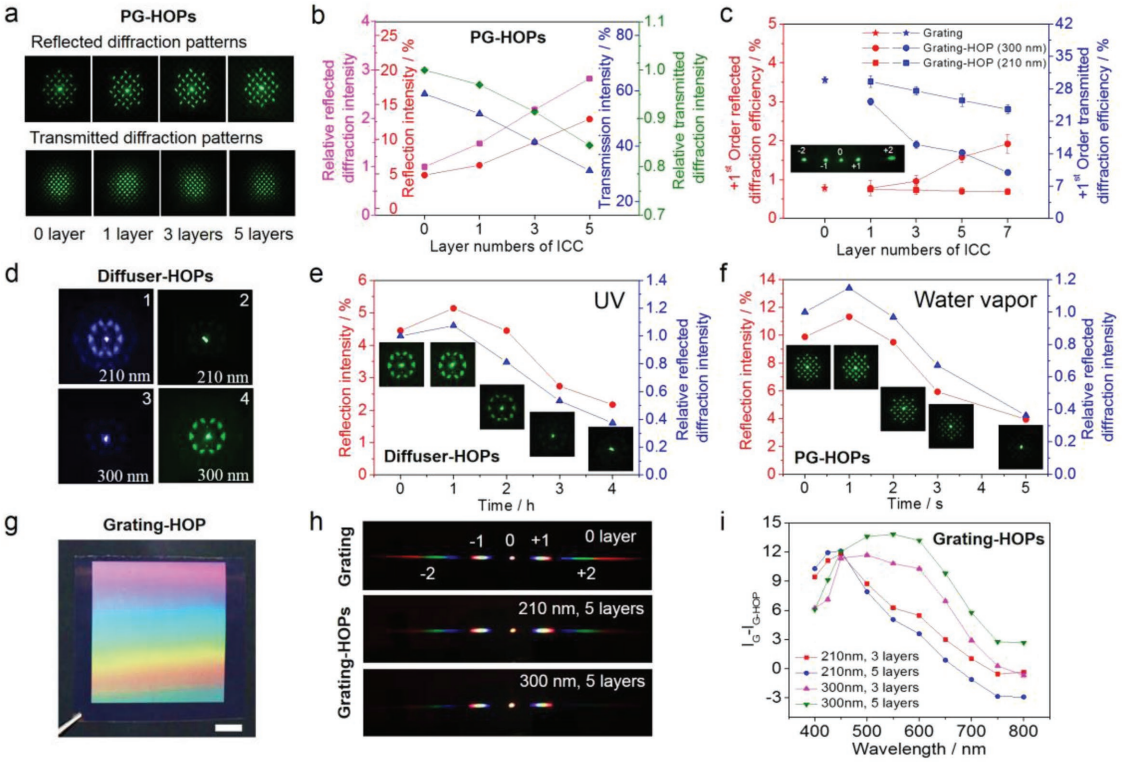

Figure 3. Diffraction performance modulation. a) Reflected (top) and transmitted (bottom) diffraction patterns of PG-HOPs with different layers of inverse colloidal crystals ($\wedge = 300$ nm) illuminated by a green laser. b) Relative diffraction, absolute reflection, and transmission intensity of PG-HOPs as a function of layer numbers of inverse colloidal crystal. c) Calculated +1st order diffraction efficiency of Grating-HOPs as a function of layer numbers. The samples were illuminated by a green laser. Insert: transmitted diffraction pattern showing different diffraction orders. d) Reflected diffraction patterns of five-layer Diffuser-HOPs with $\wedge = 210$ nm (1,2) or $\wedge = 300$ nm (3,4) illuminated by a blue (1,3) or green (2,4) laser. e,f) Reflection and diffraction intensity as a function of UV (e) and WV (f) treatment time. Inserts show the corresponding reflected diffraction patterns generated by using a green laser illumination. g) Photograph showing the split of a white light beam into its component colors of a Grating-HOP film with $\wedge = 300$ nm. Scale bar: 2 mm. h) Transmitted diffraction patterns obtained by shining a white light beam through grating and five-layer Grating-HOPs. i) The transmission intensity (+1st order) difference between grating and Grating-HOPs ($I_G - I_{Grating\text{-}HOP}$) as a function of wavelength.

or WV treatment, as confirmed by the surface SEM images (Figure S10, Supporting Information).

The diffraction properties of the Grating-HOP structures when illuminated by a white light source are also shown in Figure 3h, where the dispersed spectrum can be seen in several positive and negative diffractive orders. Compared to the plain grating, the transmitted diffraction patterns are affected by the photonic crystal transfer function which filters light in the stop-band. This is verified by analyzing the transmitted spectrum in the $m = 1$ diffracted order, which shows a consistently lower transmitted intensity where the stop-band position of the inverse opal lattice is present with varying reflected intensity as a function of the number of layers in the photonic crystal lattice (Figure 3i and Figure S11, Supporting Information).

The interplay between the photonic bandgap and 2D diffusion/diffraction affects the overall iridescence of the structures, providing a strategy to enhance spectral selectivity in biopolymer-based materials whose index contrast is low compared to inorganics and generally do not possess a complete photonic bandgap. This interplay has an impact on the reflected structural color at different angles. As an example, in the case of Diffuser-HOP/PG-HOP, the vivid yellow color is still visible as the viewing angle is changed from normal to oblique (**Figure 4**a and Figure S12a, Supporting Information) in contrast with the unpatterned silk inverse opal (seen at the edge of each element), whose color is notably blueshifted. The diffused reflectance spectra measurement (Figure 4b and Figure S12b, Supporting Information) show largely unchanged peak wavelengths as the observation angle increases. This underscores the diffusive effect of the micropatterns that results in increased viewing angles for the nanoscale lattice's structural color.

Conversely, the color varies from blue to red with the increase of observation angle for a silk diffraction grating. This simple diffractive effect is altered by adding a photonic crystal lattice and by increasing the layer numbers of the photonic crystal (Figure 4c). The observed structural color of a five-layer Grating-HOP is nearly unchanged beyond a certain angle, in contrast to the angle-dependent iridescence of a plain silk inverse opal.[28a] This provides another example of the coordinated effect between the angle dependence of the 2D grating and the photonic crystal iridescence, with the structural color from the stop-band of the photonic crystal gradually dominating the response as the lattice gets larger with the increase of the number of assembled colloidal layers.

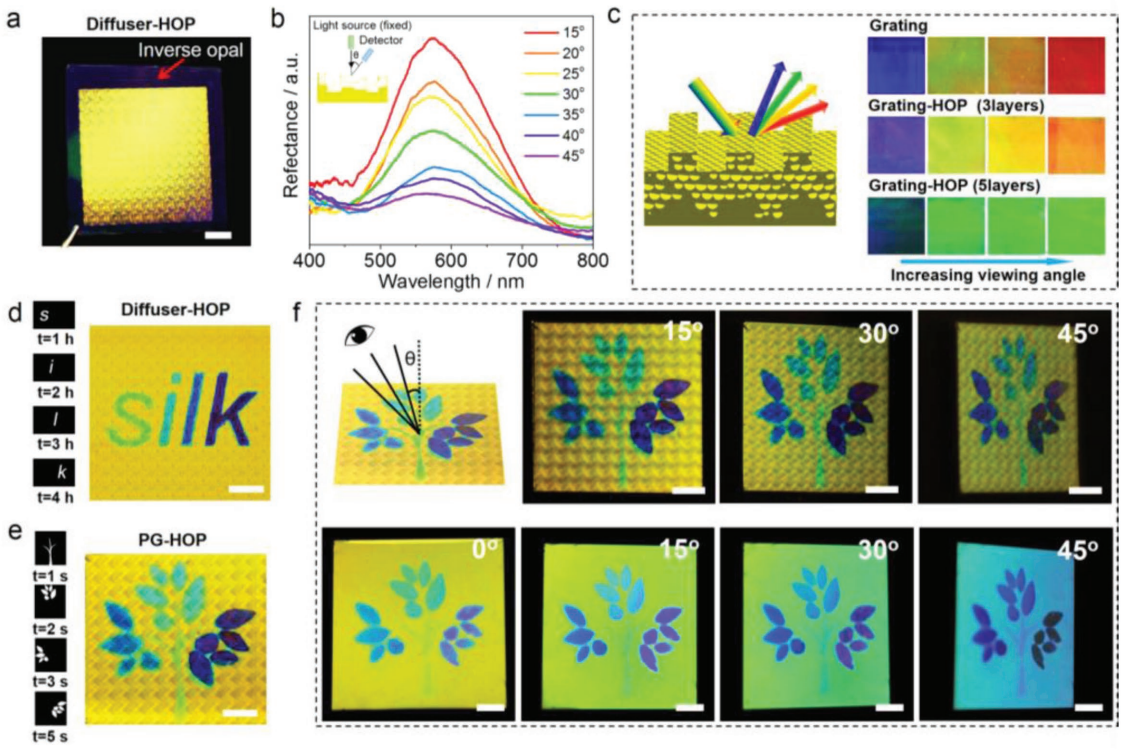

Figure 4. Structural colors of HOPs at different angles. a) Side-view photograph of Diffuser-HOP with $\wedge$ = 300 nm. The arrow indicates the inverse opal structure surrounding the Diffuser-HOP. b) Reflectance spectra of Diffuser-HOP measured under diffusive reflection mode with different detection angle (θ). insert shows the diagram of diffusive reflection measurement system. c) Schematic (left) and photographs (right) of reflected structural coloration on the grating and Grating-HOPs with $\wedge$ = 300 nm at different angles. d–f) Broad angle pattern display. (d,e) Shadow masks designs (left) and the corresponding photograph of patterned HOPs (right). (d) A "*silk*" word and (e) a tree pattern is created by selectively exposing part of Diffuser-HOP to UV light and PG-HOP to water vapor, respectively. f) Schematic diagram and photographs of the PG-HOP with a tree pattern observed at the angles from 15° to 45°. θ is defined as viewing angle. The photographs of a silk inverse opal with a tree pattern observed at different angles are also shown for comparison. Scale bars: 2 mm.

The capacity to exhibit uniform structural color over a broad viewing angle and to locally reconfigure the structural colors by selectively exposing parts of the HOPs to external stimuli and then design multicolor patterns make Diffuser-HOPs or PG-HOPs potentially viable for wide-angle pattern displays. To demonstrate this, we first generated a multicolor "*silk*" word and tree pattern by selectively exposing part of HOP to UV and WV for different times and modulating the photonic crystal lattice constant to display patterned structural color, as shown in Figure 4d,e. Structural color analysis at different angles exhibits that PG-HOP with a tree pattern (Figure 4f, top) shows little difference in structural color as the viewing angle is increased from the normal, in contrast to an unpatterned silk inverse opal where the angle-dependence of structural colors is evident (Figure 4f, bottom).

Given the coexistence of spectrally responsive functions within a unique optical element, these structures offer interesting opportunities for sensing by combining the features of photonic crystals and DOEs. Typically, photonic-crystal-based sensors work on monitoring stop-band spectral shifts, while DOEs-based sensors commonly rely on the analysis of far-field diffraction pattern changes in response to outside stimuli.[31] In this case, HOPs allow for simultaneous monitoring of stop-band spectral shifts and diffracted orders, combining the utility of both approaches. As an example, a Diffuser-HOP is used to monitor the RI changes of isopropyl alcohol (IPA)–glycerol mixtures. **Figure 5**a (and Figure S13a, Supporting Information) shows the reflectance change when the HOPs were immersed in IPA–glycerol mixtures with varying compositions. The performance of the sensor is shown in Figure 5b (and Figure S13b, Supporting Information), which plots the wavelength and reflection intensity with different volume fraction of glycerol (ϕ). An increase of the concentrations of glycerol enhances the RI of the mixed solution and results in a redshift of the stop-band, along with a decrease of reflection intensity for both HOPs with different lattice constants. The wavelength sensitivity obtained using the converted RI values is ≈263 nm/RIU (RIU, refractive index unit), comparable to some plasmonic sensor without physical swelling effect.[32] The diffraction patterns of Diffuser-HOPs as well as silk diffuser in different IPA–glycerol mixtures and the corresponding diffraction performance as a function of glycerol concentration are shown in Figure 5c,d. The diffraction intensity of Diffuser-HOP decreases with increasing glycerol concentration, the same as that of silk diffuser (Figure 5d). This dual sensing based on stop-band (wavelength shift and relative intensity change) and diffraction (intensity change) can add utility for sensing applications, pending further research to improve selectivity and sensitivity.

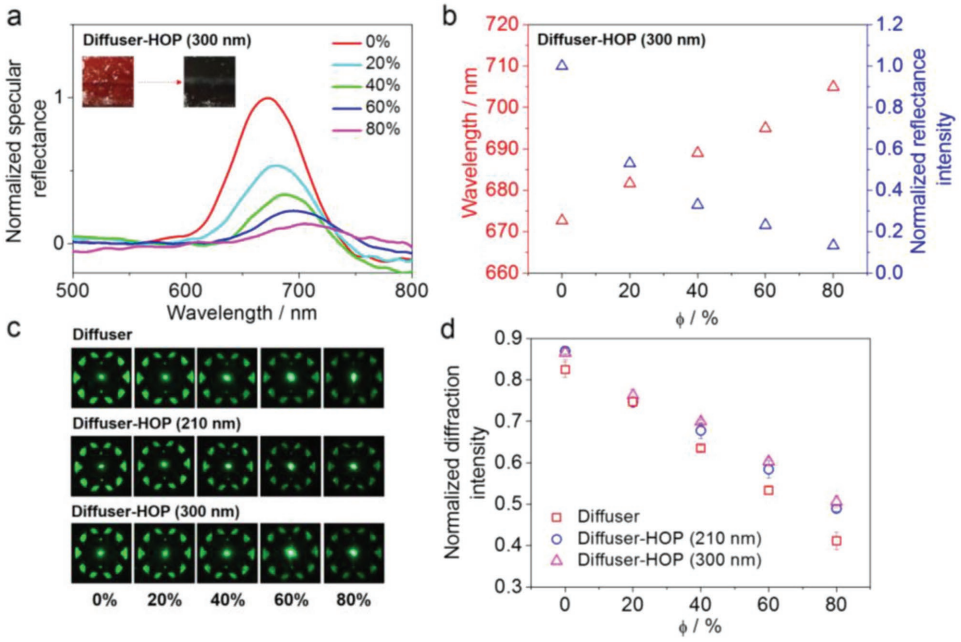

Figure 5. Applications of the HOPs for sensing. a,b) Colorimetric sensing. (a) Stop-band response of a nine-layer Diffuser-HOP with $\wedge$ = 300 nm to IPA–glycerol mixtures with varying compositions. Inserts show the structural color change when the glycerol concentration varies from ϕ = 0 to ϕ = 0.8. (b) Stop-band central wavelength and intensity as a function of the volume fraction of glycerol, ϕ. c,d) Diffraction-based sensing. (c) Transmitted diffraction patterns of diffuser and Diffuser-HOPs immersed in different IPA–glycerol mixtures. (d) Relations between normalized diffraction intensity and the volume fraction of glycerol.

In summary, we have fabricated a set of silk-fibroin-based hierarchical 3D photonic structures and demonstrated the control of their multiscale (nano, micro, and macro) features. The integration of 2D DOEs and 3D photonic crystals offers a material format that integrates reflection, diffusion, and diffraction, enabling a suite of user-defined optical properties, such as tunable diffraction performance, increased angle of view, and structural color mixing. The combination of a versatile biopolymer material format (silk fibroin), hierarchical photonic structure, and the controllability of structural color and diffraction, are promising directions for applications at the interface of photonics and biological systems. These structures could open paths for implantable devices for biomedical applications, including biodegradation process and drug delivery monitoring.[33] Moreover, the easy implementation of high reflectivity at specific wavelengths (through increasing the layer numbers of inverse colloidal crystal) and high light diffusion makes HOPs useful as potential interfaces to optoelectronic devices, to enhance their performance through increased light trapping and absorption within the devices.[15b,34] Finally, the protein nature of silk fibroin enables these structures to be used as templates that can be removed at high temperatures and readily transferred to other materials (such as Au, Al_2O_3, TiO_2 to name a few), further opening paths for photonic-crystal-based optoelectronics applications.

Supporting Information

Supporting Information is available from the Wiley Online Library or from the author.

Acknowledgements

The authors acknowledge support from the Office of Naval Research grant (N00014-16-1-2437) for this work. The authors thank Berney Peng for assistance with microscopy imaging.

Conflict of Interest

The authors declare no conflict of interest.

Keywords

diffusion/diffraction, hierarchical 3D photonic structures, multifunctionality, silk fibroin, structural color

Received: August 14, 2018
Revised: November 5, 2018
Published online: December 6, 2018

[1] a) M. Srinivasarao, *Chem. Rev.* **1999**, *99*, 1935; b) P. Vukusic, J. R. Sambles, *Nature* **2003**, *424*, 852; c) K. L. Yu, T. X. Fan, S. Lou, D. Zhang, *Prog. Mater. Sci.* **2013**, *58*, 825; d) G. T. England, J. Aizenberg, *Rep. Prog. Phys.* **2018**, *81*, 016402.
[2] H. M. Whitney, M. Kolle, P. Andrew, L. Chittka, U. Steiner, B. J. Glover, *Science* **2009**, *323*, 130.
[3] a) P. Vukusic, J. R. Sambles, C. R. Lawrence, R. J. Wootton, *Proc. R. Soc. London, Ser. B* **1999**, *266*, 1403; b) B. D. Wilts, K. Michielsen, H. De Raedt, D. G. Stavenga, *Interface Focus* **2012**, *2*, 681.
[4] A. Sweeney, C. Jiggins, S. Johnsen, *Nature* **2003**, *423*, 31.
[5] P. Vukusic, J. R. Sambles, C. R. Lawrence, *Nature* **2000**, *404*, 457.

[6] R. H. Siddique, G. Gomard, H. Holscher, *Nat. Commun.* **2015**, *6*, 6909.
[7] P. Vukusic, J. R. Sambles, C. R. Lawrence, *Proc. R. Soc. London, Ser. B* **2004**, *271*, S237.
[8] P. Vukusic, B. Hallam, J. Noyes, *Science* **2007**, *315*, 348.
[9] J. Aizenberg, A. Tkachenko, S. Weiner, L. Addadi, G. Hendler, *Nature* **2001**, *412*, 819.
[10] J. Teyssier, S. V. Saenko, D. van der Marel, M. C. Milinkovitch, *Nat. Commun.* **2015**, *6*, 6368.
[11] M. X. Kuang, J. X. Wang, L. Jiang, *Chem. Soc. Rev.* **2016**, *45*, 6833.
[12] R. A. Potyrailo, H. Ghiradella, A. Vertiatchikh, K. Dovidenko, J. R. Cournoyer, E. Olson, *Nat. Photonics* **2007**, *1*, 123.
[13] Z. W. Han, S. C. Niu, C. H. Shang, Z. N. Liu, L. Q. Ren, *Nanoscale* **2012**, *4*, 2879.
[14] A. R. Parker, H. E. Townley, *Nat. Nanotechnol.* **2007**, *2*, 347.
[15] a) A. G. Dumanli, T. Savin, *Chem. Soc. Rev.* **2016**, *45*, 6698; b) E. Armstrong, C. O'Dwyer, *J. Mater. Chem. C* **2015**, *3*, 6109.
[16] a) M. Kolle, P. M. Salgard-Cunha, M. R. J. Scherer, F. M. Huang, P. Vukusic, S. Mahajan, J. J. Baumberg, U. Steiner, *Nat. Nanotechnol.* **2010**, *5*, 511; b) Z. Gan, M. D. Turner, M. Gu, *Sci. Adv.* **2016**, *2*, e1600084; c) K. Chung, S. Yu, C. J. Heo, J. W. Shim, S. M. Yang, M. G. Han, H. S. Lee, Y. Jin, S. Y. Lee, N. Park, J. H. Shin, *Adv. Mater.* **2012**, *24*, 2375; d) M. Kolle, A. Lethbridge, M. Kreysing, J. J. Baumberg, J. Aizenberg, P. Vukusic, *Adv. Mater.* **2013**, *25*, 2239; e) Y. W. Kwon, J. Park, T. Kim, S. H. Kang, H. Kim, J. Shin, S. Jeon, S. W. Hong, *ACS Nano* **2016**, *10*, 4609; f) A. Saito, Y. Miyamura, M. Nakajima, Y. Ishikawa, K. Sogo, Y. Kuwahara, Y. Hirai, *J. Vac. Sci. Technol., B* **2006**, *24*, 3248; g) G. England, M. Kolle, P. Kim, M. Khan, P. Munoz, E. Mazur, J. Aizenberg, *Proc. Natl. Acad. Sci. USA* **2014**, *111*, 15630; h) N. Vogel, S. Utech, G. T. England, T. Shirman, K. R. Phillips, N. Koay, I. B. Burgess, M. Kolle, D. A. Weitz, J. Aizenberg, *Proc. Natl. Acad. Sci. USA* **2015**, *112*, 10845; i) M. Xiao, Z. Y. Hu, Z. Wang, Y. W. Li, A. D. Tormo, N. Le Thomas, B. Wang, N. C. Gianneschi, M. D. Shawkey, A. Dhinojwala, *Sci. Adv.* **2017**, *3*, e1701151; j) J. D. Forster, H. Noh, S. F. Liew, V. Saranathan, C. F. Schreck, L. Yang, J. G. Park, R. O. Prum, S. G. J. Mochrie, C. S. O'Hern, H. Cao, E. R. Dufresne, *Adv. Mater.* **2010**, *22*, 2939; k) S. K. Yang, N. Sun, B. B. Stogin, J. Wang, Y. Huang, T. S. Wong, *Nat. Commun.* **2017**, *8*, 1285.
[17] a) M. Schaffner, G. England, M. Kolle, J. Aizenberg, N. Vogel, *Small* **2015**, *11*, 4334; b) C. Y. Liu, Y. Long, B. Q. Yang, G. Q. Yang, C. H. Tung, K. Song, *Sci. Bull.* **2017**, *62*, 938.
[18] H. N. Umh, S. Yu, Y. H. Kim, S. Y. Lee, J. Yi, *ACS Appl. Mater. Interfaces* **2016**, *8*, 15802.
[19] a) F. G. Omenetto, D. L. KapLan, *Nat. Photonics* **2008**, *2*, 641; b) H. Tao, D. L. Kaplan, F. G. Omenetto, *Adv. Mater.* **2012**, *24*, 2824.
[20] a) N. Vogel, M. Retsch, C. A. Fustin, A. del Campo, U. Jonas, *Chem. Rev.* **2015**, *115*, 6265; b) K. R. Phillips, G. T. England, S. Sunny, E. Shirman, T. Shirman, N. Vogel, J. Aizenberg, *Chem. Soc. Rev.* **2016**, *45*, 281.
[21] a) S. Y. Lee, S. H. Kim, H. Hwang, J. Y. Sim, S. M. Yang, *Adv. Mater.* **2014**, *26*, 2391; b) I. B. Burgess, J. Aizenberg, M. Loncar, *Bioinspiration Biomimetics* **2013**, *8*, 045004.
[22] T. Ding, Q. B. Zhao, S. K. Smoukov, J. J. Baumberg, *Adv. Opt. Mater.* **2014**, *2*, 1098.
[23] a) J. X. Wang, L. B. Wang, Y. L. Song, L. Jiang, *J. Mater. Chem. C* **2013**, *1*, 6048; b) H. Kim, J. P. Ge, J. Kim, S. Choi, H. Lee, H. Lee, W. Park, Y. Yin, S. Kwon, *Nat. Photonics* **2009**, *3*, 534.
[24] a) J. W. Galusha, M. R. Jorgensen, M. H. Bartl, *Adv. Mater.* **2010**, *22*, 107; b) C. Mille, E. C. Tyrode, R. W. Corkery, *RSC Adv.* **2013**, *3*, 3109.
[25] S. M. Yang, G. A. Ozin, *Chem. Commun.* **2000**, 2507.
[26] a) M. Retsch, Z. C. Zhou, S. Rivera, M. Kappl, X. S. Zhao, U. Jonas, Q. Li, *Macromol. Chem. Phys.* **2009**, *210*, 230; b) N. Vogel, S. Goerres, K. Landfester, C. K. Weiss, *Macromol. Chem. Phys.* **2011**, *212*, 1719; c) J. R. Oh, J. H. Moon, S. Yoon, C. R. Park, Y. R. Do, *J. Mater. Chem.* **2011**, *21*, 14167; d) X. H. Meng, D. Qiu, *Langmuir* **2014**, *30*, 3019.
[27] a) S. Reculusa, S. Ravaine, *Chem. Mater.* **2003**, *15*, 598; b) S. Reculusa, P. Masse, S. Ravaine, *J. Colloid Interface Sci.* **2004**, *279*, 471.
[28] a) Y. Wang, D. Aurelio, W. Y. Li, P. Tseng, Z. Z. Zheng, M. Li, D. L. Kaplan, M. Liscidini, F. G. Omenetto, *Adv. Mater.* **2017**, *29*, 1702769; b) Y. Wang, M. Li, E. Colusso, W. Li, F. G. Omenetto, *Adv. Opt. Mater.* **2018**, *6*, 1800066.
[29] S. Kim, A. N. Mitropoulos, J. D. Spitzberg, H. Tao, D. L. Kaplan, F. G. Omenetto, *Nat. Photonics* **2012**, *6*, 817.
[30] J. P. Mondia, J. J. Amsden, D. M. Lin, L. Dal Negro, D. L. Kaplan, F. G. Omenetto, *Adv. Mater.* **2010**, *22*, 4596.
[31] D. Angeley, J. Davis, G. Reitz, *Opt. Eng.* **2006**, *45*, 043402.
[32] M. Lee, H. Jeon, S. Kim, *Nano Lett.* **2015**, *15*, 3358.
[33] Z. T. Zhou, Z. F. Shi, X. Q. Cai, S. Q. Zhang, S. G. Corder, X. X. Li, Y. S. Zhang, G. Z. Zhang, L. Chen, M. K. Liu, D. L. Kaplan, F. G. Omenetto, Y. Mao, Z. D. Tao, T. H. Tao, *Adv. Mater.* **2017**, *29*, 1605471.
[34] K. Y. Xie, M. Guo, H. T. Huang, *J. Mater. Chem. C* **2015**, *3*, 10665.

